Available online at www.sciencedirect.com
ScienceDirect
Journal of Power Sources 160 (2006) 398–406
JOURNAL OF POWER SOURCES
www.elsevier.com/locate/jpowsour

The impact of channel path length on PEMFC flow-field design

S. Shimpalee *, S. Greenway, J.W. Van Zee

Chemical Engineering Department, University of South Carolina, Columbia, SC 29208, United States

Received 17 November 2005; accepted 26 January 2006
Available online 29 March 2006

Abstract

Distributions in reactant species concentration in a PEMFC due to local consumption of fuel and local transport of water through the membrane cause distributions in current density, temperature, and water concentration in three dimensions in a PEMFC. These distributions can lead to flooding or drying of the membrane that may shorten the life of an MEA. Changing the cell's flow-field pattern to distribute the gas more evenly is one method of minimizing these stresses. This paper investigates how 200 cm^2 serpentine flow-fields with different number of gas paths, and thus different gas path lengths, affect performance and species distribution. The results show how the local temperature, water content, and current density distributions become more uniform for serpentine flow-field designs with shorter path lengths or larger number of channels. These results may be used to develop universal heuristics and dimensionless number correlations in the design of flow-fields and stacks.

Keywords: PEM; Fuel cells; Flow-field design; Fuel cell simulation; Commercial size PEMFC; Parallel computing; ES-PEMFC

1. Introduction

During operation of a proton exchange membrane fuel cell (PEMFC), hydrogen and oxygen are consumed as the fuel and air travel from inlet to outlet leading to distributions in reaction rate. This distribution of the reaction causes gradients in temperature and water production over the area of the cell. These secondary effects can feedback to change the reaction rate and can also lead to ternary effects such as local flooding when the local partial pressure of water exceeds the saturation pressure for water at the local temperature. Other ternary effects include transport distributions of water across the membrane between the anode and cathode due to electroosmosis and diffusion as well as variation of membrane conductivity due to changes in the local water activity on the anode.

Many researchers have studied the problem of water management inside PEMFCs for both steady state and transient operation [1]. However, the effect of flow-field design on PEMFC performance has received less attention. Fell et al. [2] used a single-phase isothermal CFD model of PEMFC segments to test performance of experimental flow-field designs under different humidity conditions. Greenway et al. [3] used a two-phase, non-isothermal model to study 10 cm^2 serpentine laboratory-scale flow-field patterns with different flow path lengths and inlet/outlet configurations to study cell performance and distribution uniformity. They also reported the effect of gas diffusion layer (GDL) properties on these flow-fields. Oosthuizen et al. [4] investigated mass transport under the ribs in a PEMFC using a single phase non-isothermal PEMFC model in the finite element code FIDAP to study channel to channel transport through the GDL for different GDL permeability. Experimentally, Li et al. [5] compared a serpentine pattern to a matrix of individual graphite squares and Yoon et al. [6] tested different rib widths on an 80 cm^2 cell to see the effect on performance. Commercial-size cells (~200–800 cm^2) have more pronounced effects from pressure drop, flooding distribution, and non-uniformity in temperature and current distributions due to manifolding constraints. These effects cause stability, durability, and performance problems for PEMFC stacks. Shimpalee et al. [7] explained effects seen in a patented 480 cm^2 cell under different cathode humidity conditions, but did not investigate different flow-field patterns.

The main goals of flow-field design are to increase uniformity of the current and temperature distributions at the operating conditions of interest while maintaining or improving polarization. Studies of different flow patterns will give an idea of how to optimize the flow-field design for a PEMFC stack. This optimum

* Corresponding author. Tel.: +1 803 576 6140; fax: +1 803 777 8265.
E-mail address: shimpale@engr.sc.edu (S. Shimpalee).

0378-7753/$ – see front matter © 2006 Elsevier B.V. All rights reserved.
doi:10.1016/j.jpowsour.2006.01.099

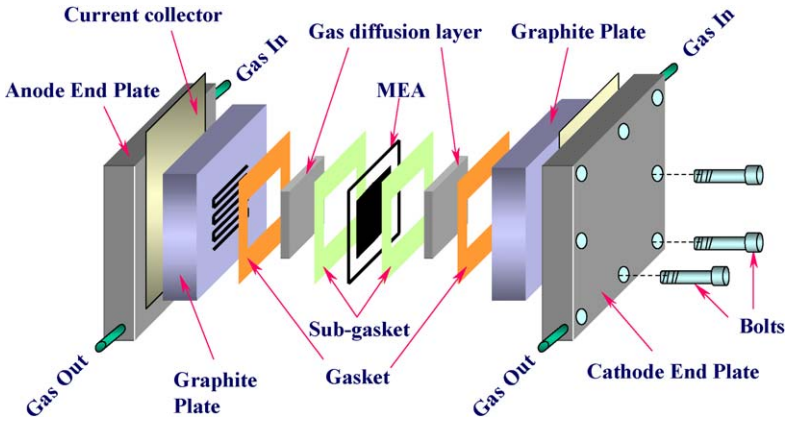

Fig. 1. Schematic of the typical PEM fuel cell used for testing of membrane and electrode assembly (MEA).

depends on temperature changes inside the system resulting from the electrochemical reaction and water phase change and it has implications for the design of the cooling/heating system. Here we consider the flow-field design, temperature change, and effects from the phase change of water on the performance of a commercial size (200 cm^2 reaction area) PEMFC performance at steady state operation.

Fig. 1 illustrates a schematic of the typical PEMFC. The cell consists of two graphite plates with machined flow channels separated by a membrane/electrode assembly (MEA). The MEA is a sandwich of a membrane between two electrodes with dispersed platinum catalysts. In this paper, we will focus on the five different 200 cm^2 flow-field patterns shown in Fig. 2. They are (a) 3-channel serpentine, (b) 6-channel serpentine, (c) 13-channel serpentine, (d) 26-channel serpentine, and (e) 26-channel complex serpentine. Geometries (a)–(d) have similar patterns, but different gas path lengths. Geometry (e) has been investigated experimentally by Buchi and Neto [8] and it has the same path length as the 26-channel serpentine flow-field. This complex geometry has been included into this study to examine the effects of the flow-field pattern. The solutions from the model will be shown and analyzed for these different flow-field configurations. The pattern of this distributed network and the effect on pressure drop will be studied and generic design principles will be developed that we hope could benefit the industry. The goal of this research is to add to the knowledge base to produce generic design information for the flow-fields that can be applied to the fuel cell stacks. Heuristic models are needed because modern day computers even with parallel processing are slow to compute optional stack designs without some intel-

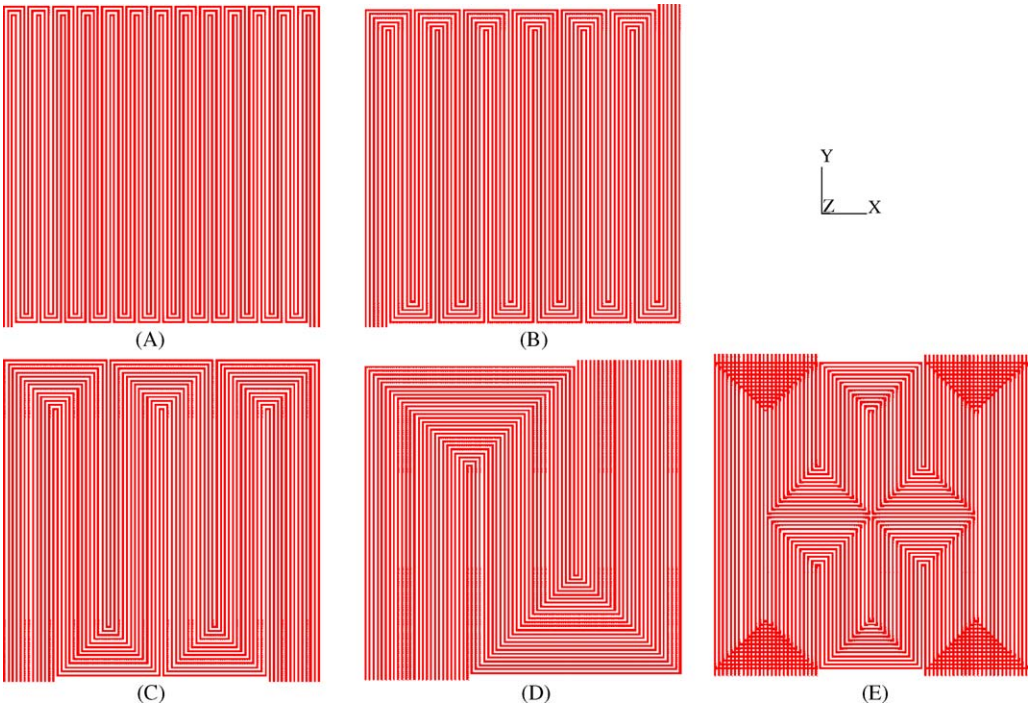

Fig. 2. Flow filed patterns of anode and cathode on 200 cm^2 PEMFC: (A) 3-channel serpentine flow-field; (B) 6-channel flow-field; (C) 13-channel flow field; (D) 26-channel flow field; (E) 26-channel complex flow-field.

ligence in the set of flow-fields considered. This study is a part of our main research goal of developing universal heuristics and dimensionless number correlations that can be used to design flow-fields and stacks. It is assumed that the development of these design techniques with CFD will require verification (of a subset of model predictions) but that proper design of experiments will expedite the development of the heuristics. That is, CFD experiments will be less costly than build-and-test experiments and they can be correlated to yield design heuristics for the next generation of PEMFCs.

2. Model development

The equations solved in this work included the conservation of mass, the Navier–Stokes equations, the species transport equations, the energy equation, and the water phase change model. Source terms for these equations used in the model were taken from Ref. [15]. In the water phase change model, when the local activity of water exceeded 1.0 water vapor was condensed to form liquid water until the local activity equaled 1.0. Conversely, if liquid water was present and the local activity of water dropped below 1.0 then liquid water was evaporated until the local activity equaled 1.0. When liquid water condensed in the region adjacent to the electrode surface, it is assumed to form a liquid film on the electrode surface. In the regions where there was a liquid film on the electrode, hydrogen and oxygen were required to dissolve in the liquid film and diffuse through the film to the electrode surface in order to react. Henry's law was used to calculate the solubility of the gases in the liquid. The thickness of this liquid film depended on the rate of condensation/evaporation and the production of water by electrochemical reaction as discussed in the appendix of Lee et al. [9].

A control volume technique based on a commercial flow solver, STAR-CD 3.150A026, was used to solve the coupled governing equations. This software was used with an add-on tool called expert system for PEMFCs (ES-PEMFC) that provided the source terms for the species transport equations, the phase change equations for water, and the heat generation equations [13]. Also, ES-PEMFC accounted for the flux of protons and water across the membrane [13].

The PEMFCs simulated in this work (shown in Fig. 2) consisted of two flow-field patterns (upper is anode and lower is cathode) separated by GDLs and an MEA. Table 1 summarizes the geometry details for each of the models and properties used in the simulation. The length of the flow path for each geometry was inversely proportional to the number of flow channels for this set of geometries. The cross-section flow areas of both geometries were 0.055 cm (height) × 0.09 cm (width). Each diffusion layer had dimensions of 0.025 cm (height) × 14.14 cm (width) × 14.14 cm (length). The number of computational cells used in the model varied with complexity of the model. For the 3-channel flow-field, the total cell number was 1.88 million cells, the 6-channel had 2.5 million computational cells, the 13-channel had 4.14 million cells, the 26-channel serpentine had 6.7 million cells, and the 26-channel complex serpentine had 5.5 million cells. The large number of computational cells used in these models could not be solved using single processor computer. Therefore, PRO-HPC, a parallel computing implementation of STAR-CD, with six nodes of a Linux cluster was used for these simulations. In the PRO-HPC implementation a domain decomposition method was used and each model was decomposed into six pieces that were sent to six different processors on the cluster for computation. Each processor's solutions were communicated to the other processors using MPICH over fast Ethernet connections.

In this study, the inlet flow velocity was controlled by stoichiometric numbers of 1.2 at anode and 2.0 at cathode and a co-flow inlet/outlet configuration was used in this study. The operating pressure was 101 kPa absolute at the exit of the cell. In the model, the system pressure was calculated every iteration to get the correct inlet pressure, velocity, and species' component corresponding to inlet stoichiometry and humidification. For temperature predictions, the bi-polar plate temperature was maintained at 70 °C. The inlet humidity in this study for both the anode and cathode corresponded to 80 and 70 °C dew point temperatures with 100% relative humidity, respectively. Note that the conditions used in this study were the optimum PEMFC operating conditions found from internal experimental studies. All the parameters used (e.g., oxygen exchange current density, hydrogen exchange current density, and gas diffusion media

Table 1
Geometry details, GDL properties, and MEA properties

	3-channel	6-channel	13-channel	26-channel	26-channel complex
Channel width (mm)	0.9	0.9	0.9	0.9	0.9
Channel height (mm)	0.55	0.55	0.55	0.55	0.55
Channel length (mm)	3700	1800	840	420	420
Rib-spacing width (mm)	0.9	0.9	0.9	0.9	0.9
GDL thickness (μm)	250	250	250	250	250
GDL permeability (m^2)	1.0E−12	1.0E−12	1.0E−12	1.0E−12	1.0E−12
GDL porosity	0.7	0.7	0.7	0.7	0.7
GDL thermal conductivity (W/m K)	0.213	0.213	0.213	0.213	0.213
GDL diffusion adjustment (%)	50	50	50	50	50
MEA thickness (μm) (including 12.5 μm thickness of catalyst layer)	50	50	50	50	50
MEA thermal conductivity (W/m K)	0.147	0.147	0.147	0.147	0.147
Dry membrane density (g/cm^3)	2.0	2.0	2.0	2.0	2.0
Equivalent weight of dry membrane (g/mol)	1100	1100	1100	1100	1100

Table 2
Operating conditions

	3- channel	6-channel	13-channel	26-channel	26-channel complex
Anode channel inlet conditions					
Gas	H_2	H_2	H_2	H_2	H_2
Stoichiometry	1.2	1.2	1.2	1.2	1.2
Inlet temperature (°C)	80	80	80	80	80
Inlet relative humidity (%)	100	100	100	100	100
Cathode channel inlet conditions					
Gas	Air	Air	Air	Air	Air
Stoichiometry	2.0	2.0	2.0	2.0	2.0
Inlet temperature (°C)	70	70	70	70	70
Inlet relative humidity (%)	100	100	100	100	100
Operating conditions					
Exit pressure (kPa)	101	101	101	101	101
Hydrogen exchange current density (A/cm^2)	0.5	0.5	0.5	0.5	0.5
Oxygen exchange current density (A/cm^2)	0.05	0.05	0.05	0.05	0.05
Open circuit voltage (V)	0.98	0.98	0.98	0.98	0.98
Cell temperature (°C)	70	70	70	70	70

properties) were shown in Tables 1 and 2. In this work, we considered the effect of flow-field configuration or the path length on the PEM fuel cell performance. The results of local current density, electrochemical variables, temperature, and pressure drop with different flow-field configurations were compared and discussed further.

3. Results and discussion

Fig. 3 shows the polarization curves of the five flow-fields at the conditions specified in Table 2. The 13-channel flow-field has the highest performance in the IR region (i.e. cell voltages between 0.6 and 0.75) and the mass transfer limited region (i.e. cell voltages below 0.6) followed in order by the 26-channel complex flow-field, the 26-channel flow-field, the 6-channel flow-field, and 3-channel flow-field. In the kinetic region (i.e. cell voltages above 0.75), the 3-channel flow-field has the best performance. This high performance in the kinetic region for the 3-channel flow-field is related to pressure effects in the flow-field as will be discussed below. However, at current densities above 1.0 A/cm^2, the performances of both the 3-channel and 6-channel flow-fields drop significantly compared to the other flow-fields. This could be due to the effect of path length on the local performance. In order to investigate which flow-field or path length gives the optimum solution, the distributions of other variables will be studied.

Some developers try to engineer their flow-fields to give uniform membrane hydration at conditions as close to saturated as possible without flooding. Maintaining uniform distribution of membrane water content is one method of extending the lifetime of PEMFC systems, because this reduces the formation of local hot spots and flooding that can stress and damage MEAs. Fig. 4 shows the average membrane water content (λ) at each current density for the flow-fields in this study. The membrane water content indicates how well membrane is hydrated and is the key to low membrane resistance. Fig. 4 reveals that the 3-channel flow-field has the highest membrane water content for all cur-

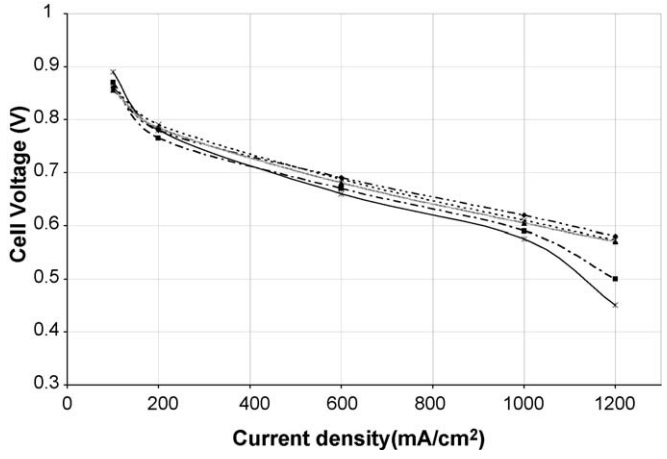

Fig. 3. The performance curves of these five flow-filed configurations with the condition of 80 °C/70 °C dew point at 1.2/2.0 stoich with 101 kPa system pressure and 70 °C cell temperature: 3-channel (*); 6-channel (■); 13-channel (♦); 26-channel (▲); 26-channel-complex (×).

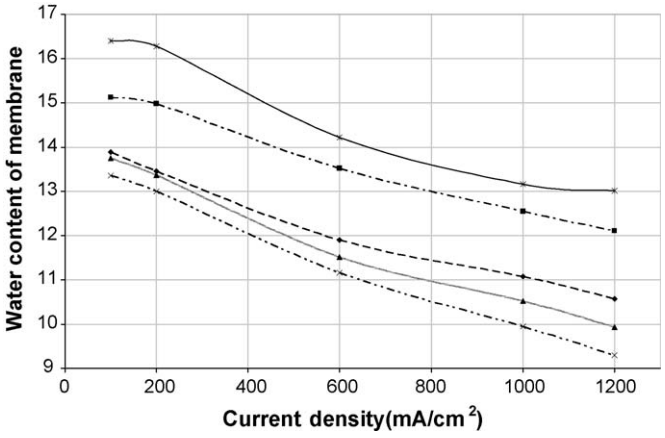

Fig. 4. Average value of water content of membrane at each point on performance curves of these five flow-field configurations: 3-channel (*); 6-channel (■); 13-channel (♦); 26-channel (▲); 26-channel-complex (×).

rent densities, but as current density increases the membrane water content decreases. The decrease in membrane water content at increasing current density occurs due to the increase in net water transport from anode to cathode with increasing current density. The increased net water transport from anode to cathode results in drying of the membrane because the hydration state of the membrane is a stronger function of anode water activity than cathode water activity [10–12]. Membrane water content has a maximum of 14.0 for a water vapor equilibrated membrane, but for a membrane equilibrated with liquid water this value can reach 22.0 [14]. For the 3-channel and 6-channel flow-fields the membrane water content is above 14.0 for low current densities, which indicates that these flow-fields have significant fraction of liquid water. The presence of liquid water could explain why the overall performance of this 3- and 6-channel flow-fields show the lowest performance even though they have high values of membrane water content. For the flow-fields with shorter path length (i.e. 13-channel, 26-channel, and 26-channel complex), their performances are consistent with the membrane water content profile. The overall performance of 13-channel flow-field is higher than both of the 26-channel flow-fields because it has higher overall membrane water content at each average current density.

The water content of the membrane is linearly related to the proton conductivity of the membrane such that higher membrane water content leads to higher proton conductivity. The voltage loss caused by the resistance of the membrane to proton transport can be calculated at each point on the polarization curve as shown in Fig. 5. This figure shows increasing potential loss with increasing of averaged current density. This behavior is intuitive based on the results for membrane water content shown in Fig. 4. The most striking result from this plot is that the membrane in these cells is only responsible for a maximum of 10 mV of the total voltage drop in the cell. At each current density, the difference in membrane voltage drop between the different flow-fields is only around 1 mV even when the membrane water content is 30% different. This indicates that if flows are well-humidified then the flow-field should be designed more for eliminating flooding conditions than trying to have a perfectly uniform membrane water content distribution.

The effect of oxygen concentration in the cathode on PEMFC polarization is reflected in the kinetic overpotential. Fig. 6 shows the area averaged kinetic overpotential as function of current density. This figure shows average value of kinetic overpotential at each point on performance curves shown in Fig. 3. The 3-channel flow-field has the smallest overpotential at very low current densities because it has the highest partial pressure of reacting gases. At low current densities the amount of water of produced in the cathode is also small. This combination of effects leads to a high partial pressure of oxygen in the cathode for flow-fields with longer path lengths even though the oxygen stoichiometry remains the same. This explains why the 3-channel flow-field has is the highest performance in this region as shown in Fig. 3. For all flow-fields, when the average current density increases the kinetic overpotential also increases. In the IR and mass transfer regions, the 13- and 26-channel flow-fields have smaller kinetic overpotentials than the 3- and 6-channel flow-fields. When the average current density is beyond 1000 mA/cm^2, the value of overpotential is significantly increased for the 3- and 6-channel flow-fields due to mass transfer. With longer path length flow-fields like 3-channel and 6-channel, the decreasing of gases' partial pressure and the accumulation of water are very intense especially in the last half of the reaction area.

The pressure drop across the flow-field is an extremely important metric for PEMFC system design because it will define the types of compressors or blowers that are needed and the pressure drop will also have an impact on the electrochemistry in the cell. Fig. 7 shows the effect of flow channel path lengths on the membrane water content and cathode pressure drops at average current density of 1000 mA/cm^2. This figure shows that pressure drop and water content increase with the increase of path length. The pressure drop decreases as the number of flow channels increases because there are more parallel paths that the flow can take. As the total pressure increases and the mole

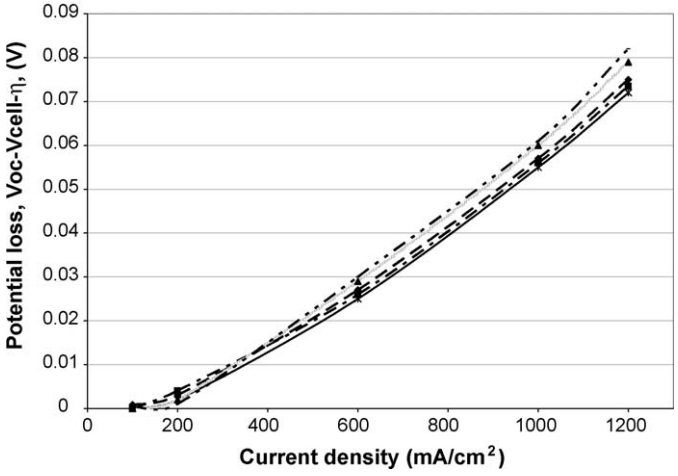

Fig. 5. Ohmic potential loss causing by membrane conductivity at each point on performance curves of these five flow-field configurations: 3-channel (*); 6-channel (■); 13-channel (♦); 26-channel (▲); 26-channel-complex (×).

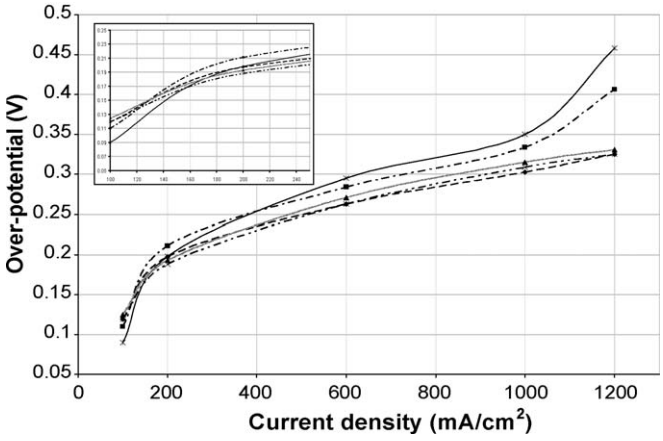

Fig. 6. Average value of kinetic overpotential at each point on performance curves of these five flow-field configurations: 3-channel (*); 6-channel (■); 13-channel (♦); 26-channel (▲); 26-channel-complex (×).

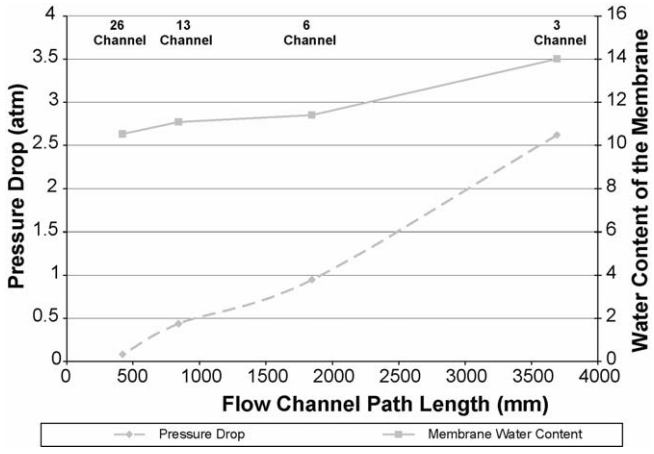

Fig. 7. The effect of flow channel path length from different flow-fields on membrane water content and cathode pressure drop at average current density of 1000 mA/cm^2.

fraction of water remains constant, then the partial pressure of water, and thus the activity, increases. The increasing activity of water will thus raise the membrane water content.

The distribution of reaction rates across the electrode surface causes distributions in temperature and other electrochemical variables in a PEMFC. Distribution uniformity is important for minimizing the material stresses on the MEA so that its lifetime will be improved. Fig. 8 shows the local temperature over the anode membrane surface at 1000 mA/cm^2. The temperature of the bipolar plate in all simulations is set at 70 °C (343 K) and the source term for the heat of reaction is placed at the cathode/membrane interface. The simulations show the electrode temperature near the inlet region for all cases is near 80 °C. The temperature then drops to around 75 °C in the middle of the flow-field and maintains that temperature through the exit region. The 26-channel complex flow-field has a temperature distribution that is more uniform than the other co-flow flow-fields including the other 26-channel flow-field. This could be due to the special matching of the maximum hydrogen and oxygen concentrations at the inlet for co-flow configurations. Furthermore, the average temperature between 13-channel and 26-channel is only slightly different. This means that there is a limit to how much the temperature uniformity can be adjusted by changing the flow path length. It is noted that the temperature under the rib areas is lower than the adjacent channel areas. This is because the heat produced in the area under ribs is more easily transferred to the graphite block compared to heat produced in the area under the channels.

Fig. 9 shows the average temperature on the anode membrane surface as a function of the average current density. The temperature increases with increasing current density because of higher reaction rate. As seen in Fig. 8, there are small differences in average temperature at the cathode/membrane interface for different flow-fields, but with the 70 °C uniform plate temperature boundary condition these differences are only around 1 °C. The insert bar graph shows the temperature difference between the maximum and minimum local temperatures for different flow-fields at an average current density of 1000 mA/cm^2. This graph shows that longer path length flow-fields have larger temperature ranges than shorter path length flow-fields. By looking at the temperature distributions in Fig. 8, it can be observed that the difference in average temperatures is mostly caused by the hot spot in the entrance region. The size of the hot spot decreases as the number of channels increases and the entrance region is

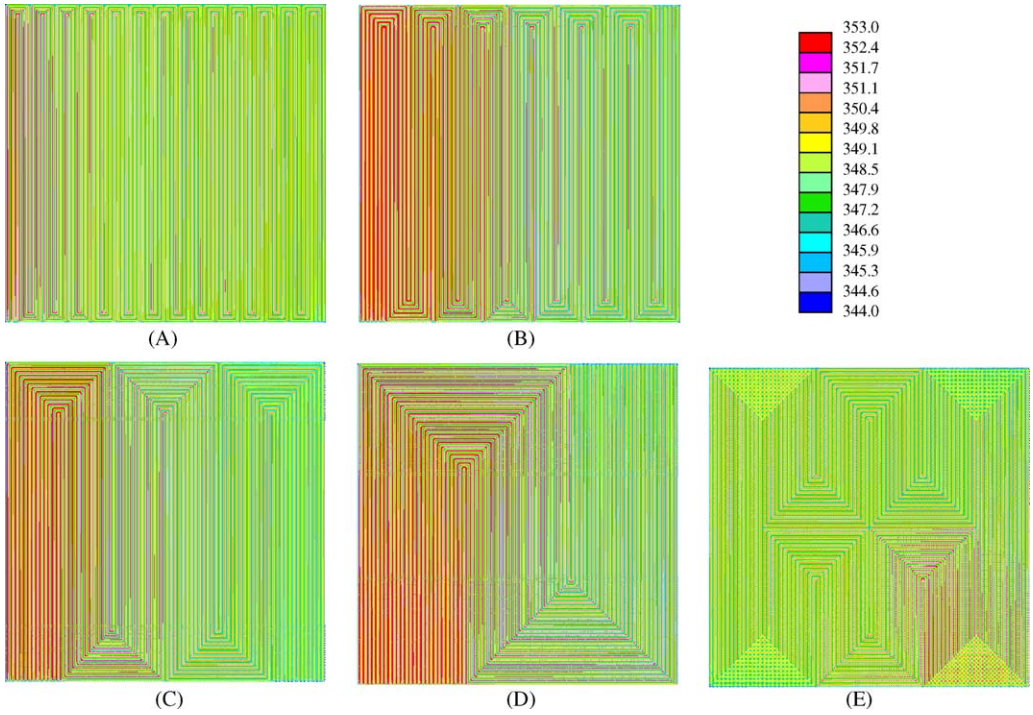

Fig. 8. Temperature (K) distributions on anode MEA surface at I_{avg} = 1000 mA/cm^2: (A) 3-channel serpentine flow-field; (B) 6-channel flow-field; (C) 13-channel flow field; (D) 26-channel flow field; (E) 26-channel complex flow-field.

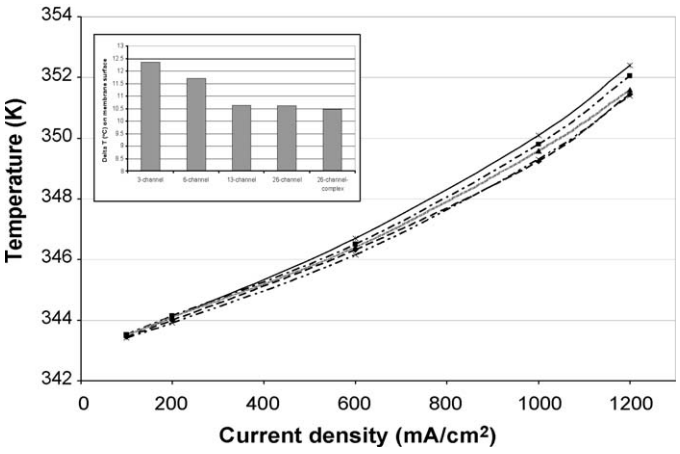

Fig. 9. Average value of temperature on membrane surface at each point on performance curves of these five flow-field configurations. Bar graph shows maximum temperature difference on membrane surface at $I_{avg} = 1000\,mA/cm^2$: 3-channel (*); 6-channel (■); 13-channel (♦); 26-channel (▲); 26-channel-complex (×).

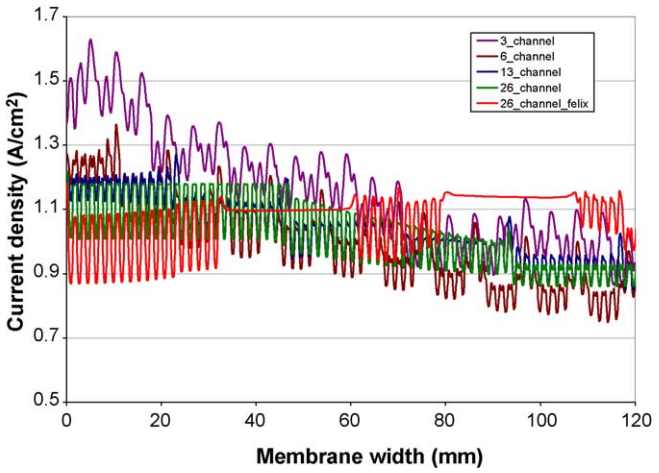

Fig. 11. Current density plots along centerline of MEA from inlet toward outlet (i.e. at x-direction at $y = 7.07$ cm) at $I_{avg} = 1000\,mA/cm^2$ for five different flow-fields.

spread over more area. The average temperature between 13- and 26-channel flow-fields are only slightly different which suggests that there is a limit to how uniform the temperature profile can be made by increasing the number of flow channels.

Fig. 10 shows current density distribution on MEA surface of the 3-, 6-, 13-, and 26-channel serpentine, and the 26-channel complex serpentine flow paths, respectively. The 13-channel flow-field has a higher cell voltage than other flow-fields. The 3-, 6-, 13-, and 26-channel flow-fields give cell voltages of 0.575, 0.590, 0.620 and 0.605 V, respectively. One important aspect of these distributions is the range of current variation. The distributions in Fig. 10 show that the 26-channel flow-fields have the least variation in current density. The 3-, 6-, 13-, and 26-channel flow-fields have differences between the maximum and minimum local current densities of 840, 700, 430, and 370 mA/cm^2, respectively. The variability in the current density can cause local variations in the cell temperature, membrane conductivity, and water concentration. The non-uniformities then cause mechanical stresses on the system that reduces MEA lifetime.

Fig. 11 shows further detail of above contours on the uniformity aspect. This figure presents the current density plots

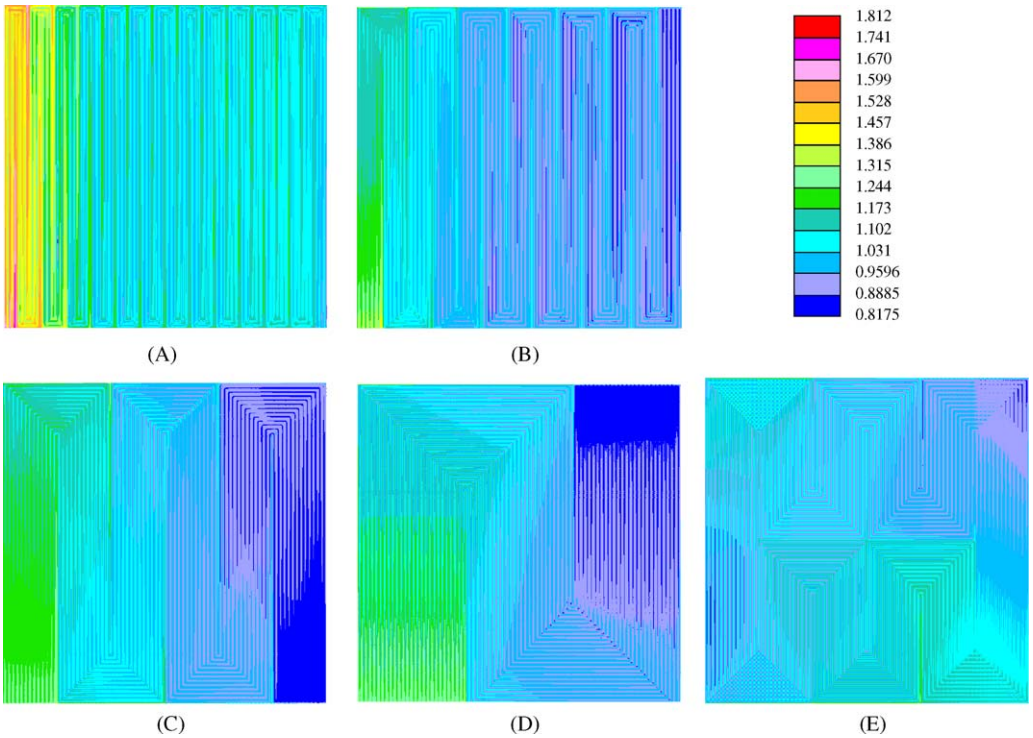

Fig. 10. Current density (A/cm^2) distributions at $I_{avg} = 1000\,mA/cm^2$: (A) 3-channel serpentine flow-field; (B) 6-channel flow-field; (C) 13-channel flow field; (D) 26-channel flow field; (E) 26-channel complex flow-field.

Table 3
Conclusions of path length analysis on a square 200 cm^2 PEMFC with three different current densities (A/cm^2) at 1.2/2.0 stoich flow rate

Flow-field type	3-channel			6-channel			13-channel			26-channel			26-complex		
Average current density (A/cm^2)	0.2	0.6	1.0	0.2	0.6	1.0	0.2	0.6	1.0	0.2	0.6	1.0	0.2	0.6	1.0
Channel length (cm)	369	369	369	184	184	184	84	84	84	42.1	42.1	42.1	41.5	41.5	41.5
Anode inlet pressure (kPa g)	17.9	40.3	59.3	4.60	13.4	12.1	1.92	3.68	14.0	0.54	1.05	1.27	0.62	1.15	1.54
Anode inlet velocity (m/s)	6.81	15.6	21.6	4.17	10.9	16.3	2.26	6.79	11.3	1.13	3.39	5.66	1.13	3.39	5.66
Anode inlet H_2 mole fraction	0.61	0.67	0.71	0.56	0.59	0.62	0.54	0.54	0.54	0.54	0.54	0.54	0.54	0.54	0.54
Anode inlet H_2O mole fraction	0.39	0.33	0.29	0.44	0.41	0.38	0.46	0.46	0.46	0.46	0.46	0.46	0.46	0.46	0.46
Cathode inlet pressure (kPa g)	63.0	169	266	20.0	58.7	96.1	8.11	24.3	43.6	2.03	4.05	8.11	2.03	4.05	8.11
Cathode inlet velocity (m/s)	14.2	23.7	28.2	10.5	22.0	28.5	6.04	15.0	20.8	3.27	9.55	15.1	3.27	9.55	15.1
Cathode inlet O_2 mole fraction	0.17	0.19	0.19	0.16	0.17	0.18	0.15	0.16	0.16	0.15	0.15	0.15	0.15	0.15	0.15
Cathode inlet N_2 mole fraction	0.64	0.70	0.72	0.59	0.64	0.67	0.57	0.60	0.62	0.55	0.56	0.57	0.55	0.56	0.57
Cathode inlet H_2O mole fraction	0.19	0.11	0.09	0.25	0.19	0.15	0.28	0.24	0.22	0.30	0.29	0.28	0.30	0.29	0.28
Cell voltage (V)	0.78	0.66	0.57	0.77	0.67	0.59	0.78	0.69	0.62	0.79	0.68	0.60	0.79	0.68	0.60
Current density (A/cm^2) variation (max − min)	0.25	0.47	0.84	0.2	0.4	0.69	0.15	0.29	0.42	0.16	0.27	0.36	0.16	0.26	0.37
Membrane water content	16.3	14.2	13.2	15	13.5	12.5	13.4	11.9	11.1	13.3	11.5	10.5	12.9	11.3	10
Kinetic over potential (V) (anode + cathode)	0.2	0.3	0.35	0.2	0.28	0.33	0.2	0.26	0.3	0.19	0.27	0.31	0.18	0.26	0.3
Temperature (°C) variation	3.1	7.2	12.3	2.9	7.0	11.7	2.32	5.69	10.6	2.23	5.4	10.6	1.56	5.3	10.4

along the centerline of MEA from inlet toward outlet (i.e. at $y = 7.07$ cm and plot along x-direction from 0 to 14.14 cm.). The plot of each flow-field shows regular peaks and valleys caused by different rates of heat transfer in the reaction areas under the flow paths and under ribs. Fig. 11 shows that the current density under the rib areas is higher than under the adjacent channel areas. This higher current density under the ribs is caused by local temperature as explained in Fig. 8. Therefore, the lower temperature under the ribs compared to under the channels increases the membrane water content due to the reduction of saturation pressure of water; thus, raising local performance. In order to reduce variations in current density between channel and rib areas the material and thermal properties of materials including bipolar plate, GDL, and MEA could be further studied.

From above results, it is noted that the results between 26-channel conventional serpentine and 26-channel complex serpentine are about similar for all parameters and their uniformity. This can be concluded that with the same path length, the performance and other variables will be the same and this has slightly effect by flow-field pattern. In these flow-field studies, it shows that 26-channel give the most uniformity than other flow-fields. Furthermore, the 26-channel give the least pressure drop compare to the other flow-fields.

The simulations show that the 13-channel gives the best performance for a single 200 cm^2 PEMFC. However, for making a PEMFC stack, the 26-channel flow-field may be the optimal choice to use rather 13-channel due to more current density uniformity and a lower pressure drop. Table 3 is the summary of these studies discussed above for three points of the *V–I* curve (i.e. 200, 600, and 1000 mA/cm^2) and it shows the comparison of these flow-filed bases on channel length, cell voltage, current variation, temperature variation, membrane water content, and pressure drop.

4. Conclusion

The effect of flow-field path length and pattern on the distribution of current, temperature, and electrochemical variables on commercial-size PEMFC performance was studied using the ES-PEMFC model. The models used a commercial computational fluid dynamics solver, STAR-CD, and its PEMFC model add-on coded by University of South Carolina for computation in steady-state, multi-species, multi-phase, and non-isothermal schemes. The patterns studied were 200 cm^2 reaction area cells with 3-, 6-, 13- and 26-channel flow-fields.

It is concluded that changing flow-field configuration by varying path length of PEMFC by changing the number of parallel channels can affect its performance and uniformity. The shorter path length gives more uniform current density distribution and less condensed liquid water than the longer path. However, from an overall performance aspect, the 13-channel flow-field gave a slight advantage over the 26-channel flow-field due mostly to small differences in membrane hydration. With similar path length, the performance appears to be relatively independent of its configuration for the 26-channel cases that were tested. Therefore, the path length of a PEMFC flow-field is one of the

major variables for optimizing the performance, efficiency, and durability of PEMFC.

Acknowledgements

This work was supported by the companies in the National Science Foundation of Industrial/University Collaborative Research Center for Fuel Cells (NSF-I/UCRC for Fuel Cells, http://www.fuelcells.sc.edu) at the University of South Carolina. We would like to gratefully acknowledge the CD-adapco group for providing the CFD software.

References

[1] C.Y. Wang, Chem. Rev. 104 (2004) 4727–4766.
[2] S. Fell, J. Roth, B. Steidle, D. Baker, W. Gu, M. Mathias, M. Schoeneweiss, VDI Berichte (2002) 579–600.
[3] S. Greenway, S. Shimpalee, J.W. Van Zee, Presented at the 21st Meeting of the Electrochemical Society, Philidephia, PA, May 2002 (Abstract #1135).
[4] P.H. Oosthuizen, L. Sun, K.B. McAuley, Appl. Thermal Eng. 25 (2005) 1083–1096.
[5] P.W. Li, S.P. Chen, M.K. Chyu, J. Power Sources 140 (2005) 311–318.
[6] Y.G. Yoon, W.Y. Lee, G.G. Park, T.H. Yang, C.S. Kim, Electrochim. Acta 50 (2004) 709–712.
[7] S. Shimpalee, S. Greenway, D. Spuckler, J.W. Van Zee, J. Power Sources 135 (2004) 79–87.
[8] F.N. Buchi, R.P. Neto, Presented at the 201st Meeting of the Electrochemical Society, Philidelphia, PA, May 2002 (Abstract #821).
[9] W.K. Lee, S. Shimpalee, J.W. Van Zee, J. Electrochem. Soc. 150 (2003) A341–A348.
[10] F.N. Buchi, G.G. Scherer, J. Electrochem. Soc. 148 (2001) A183–A188.
[11] F.N. Buchi, G.G. Scherer, J. Electroanal. Chem. 404 (1996) 37–43.
[12] F.N. Buchi, S. Srinivasan, J. Electrochem. Soc. 144 (1997) 2767–2772.
[13] ES-PEMFC Methodology and Tutorial Manual, CD adapco Group, http://www.adapco.com.
[14] T.E. Springer, T.A. Zawodzinski, S. Gottesfeld, J. Electrochem. Soc. 138 (1991) 2334.
[15] S. Shimpalee, S. Dutta, Numer. Heat Transfer Part A 38 (2000) 111.